THE JOURNAL OF PHYSICAL CHEMISTRY A
A JOURNAL OF THE AMERICAN CHEMICAL SOCIETY

pubs.acs.org/JPCA

Article

High-Level Systematic Ab Initio Comparison of Carbon- and Silicon-Centered S_N2 Reactions

Attila Á. Dékány, Gyula Z. Kovács, and Gábor Czakó*

Cite This: *J. Phys. Chem. A* 2021, 125, 9645−9657

Read Online

ACCESS | Metrics & More | Article Recommendations | Supporting Information

ABSTRACT: We characterize the stationary points along the Walden inversion, front-side attack, and double-inversion pathways of the $X^- + CH_3Y$ and $X^- + SiH_3Y$ [X, Y = F, Cl, Br, I] S_N2 reactions using chemically accurate CCSD(T)-F12b/aug-cc-pV*n*Z [*n* = D, T, Q] levels of theory. At the carbon center, Walden inversion dominates and proceeds via prereaction ($X^-\cdots H_3CY$) and postreaction ($XCH_3\cdots Y^-$) ion-dipole wells separated by a usually submerged transition state $(X-H_3C-Y)^-$, front-side attack occurs over high barriers, double inversion is the lowest-energy retention pathway for X = F, and hydrogen- ($F^-\cdots HCH_2Y$) and halogen-bonded ($X^-\cdots YCH_3$) complexes exist in the entrance channel. At the silicon center, Walden inversion proceeds through a single minimum $(X-SiH_3-Y)^-$, the front-side attack is competitive via a usually submerged transition state separating pre- and postreaction minima having X−Si−Y angles close to 90°, double inversion occurs over positive, often high barriers, and hydrogen- and halogen-bonded complexes are not found. In addition to the S_N2 channels ($Y^- + CH_3X/SiH_3X$), we report reaction enthalpies for proton abstraction ($HX + CH_2Y^-/SiH_2Y^-$), hydride substitution ($H^- + CH_2XY/SiH_2XY$), $XH\cdots Y^-$ complex formation ($XH\cdots Y^- + {}^1CH_2/{}^1SiH_2$), and halogen abstraction ($XY + CH_3^-/SiH_3^-$ and $XY^- + CH_3/SiH_3$).

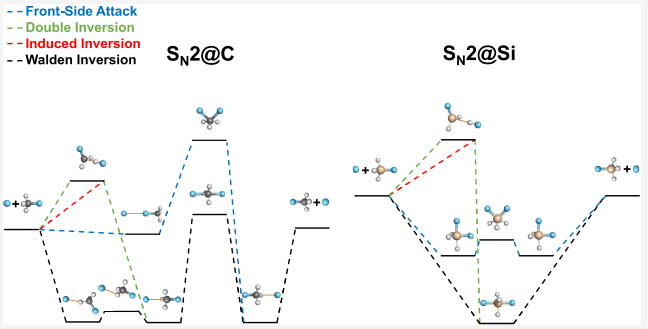

1. INTRODUCTION

Since Walden's discovery in 1896,[1] bimolecular nucleophilic substitution (S_N2) reactions at a tetrahedral carbon center have been widely studied both experimentally and theoretically.[2−35] The prototypes of these reactions are $X^- + CH_3Y \rightarrow Y^- + CH_3X$, where X, Y = F, Cl, Br, I. The $X^- + CH_3Y$ S_N2 reactions usually proceed with Walden inversion on a double-well potential along the collinear X−C−Y arrangement via a prereaction ion-dipole complex ($X^-\cdots H_3CY$), a central transition state $(X-CH_3-Y)^-$, and a postreaction ion-dipole complex ($XCH_3\cdots Y^-$). In addition to the well-known Walden-inversion mechanism, it was earlier recognized[2] that S_N2 reactions may occur via a high-energy front-side attack transition state $(XYCH_3)^-$, where the XCY angle is around 80°.[11,20,22,23,25,26,36−38] Furthermore, recent studies revealed that hydrogen- ($X^-\cdots HCH_2Y$)[15,18,20] and halogen-bonded ($X^-\cdots YCH_3$)[24,29,33] complex formations may also play key roles in carbon-centered S_N2 reactions. Moreover, reaction dynamics simulations uncovered a double-inversion pathway for the $F^- + CH_3Cl$ S_N2 reaction, which provides products with retention of the initial configuration via double-inversion ($FH\cdots CH_2Cl^-$) and Walden-inversion $(F-CH_3-Cl)^-$ transition states.[21] Since the discovery of double inversion in 2015,[21] this mechanism has been identified in several other S_N2 reactions both in the gas[22,23,26,27] and solution[39,40] phases. In addition to the widely studied carbon-centered systems, the S_N2 reaction can also occur at the silicon center.[41−56] Even though silicon is below carbon in the periodic table, it is well established in the literature[41−56] that silicon-centered S_N2 reactions are quite different from their carbon-centered analogues. The $X^- + SiH_3Y$ reactions can be characterized by a single-well Walden-inversion potential featuring a deep minimum corresponding to the penta-covalent $(X-SiH_3-Y)^-$ complex. Furthermore, due to the large size of the Si atom, at the silicon center, the front-side attack transition states $(XYSiH_3)^-$ are also usually submerged, opening barrierless retention pathways that may compete with Walden inversion.[41,47−50] Despite the interesting features of silicon-centered S_N2 reactions, these systems are less studied than the carbon-centered analogues. In the case of the $X^- + SiH_3Y$-type reactions, mostly the $Cl^- + SiH_3Cl$ (refs 41, 43−50, 53, 54, 56) identity process is investigated in addition to the few studies on $F^- + SiH_3F$ (refs 41, 48, 56). The theoretical studies on these reactions usually used density functional theory with triple-zeta basis sets to characterize the stationary points,[43−47,50,54,56] and

Received: August 26, 2021
Revised: October 13, 2021
Published: October 28, 2021

https://doi.org/10.1021/acs.jpca.1c07574
J. Phys. Chem. A 2021, 125, 9645−9657

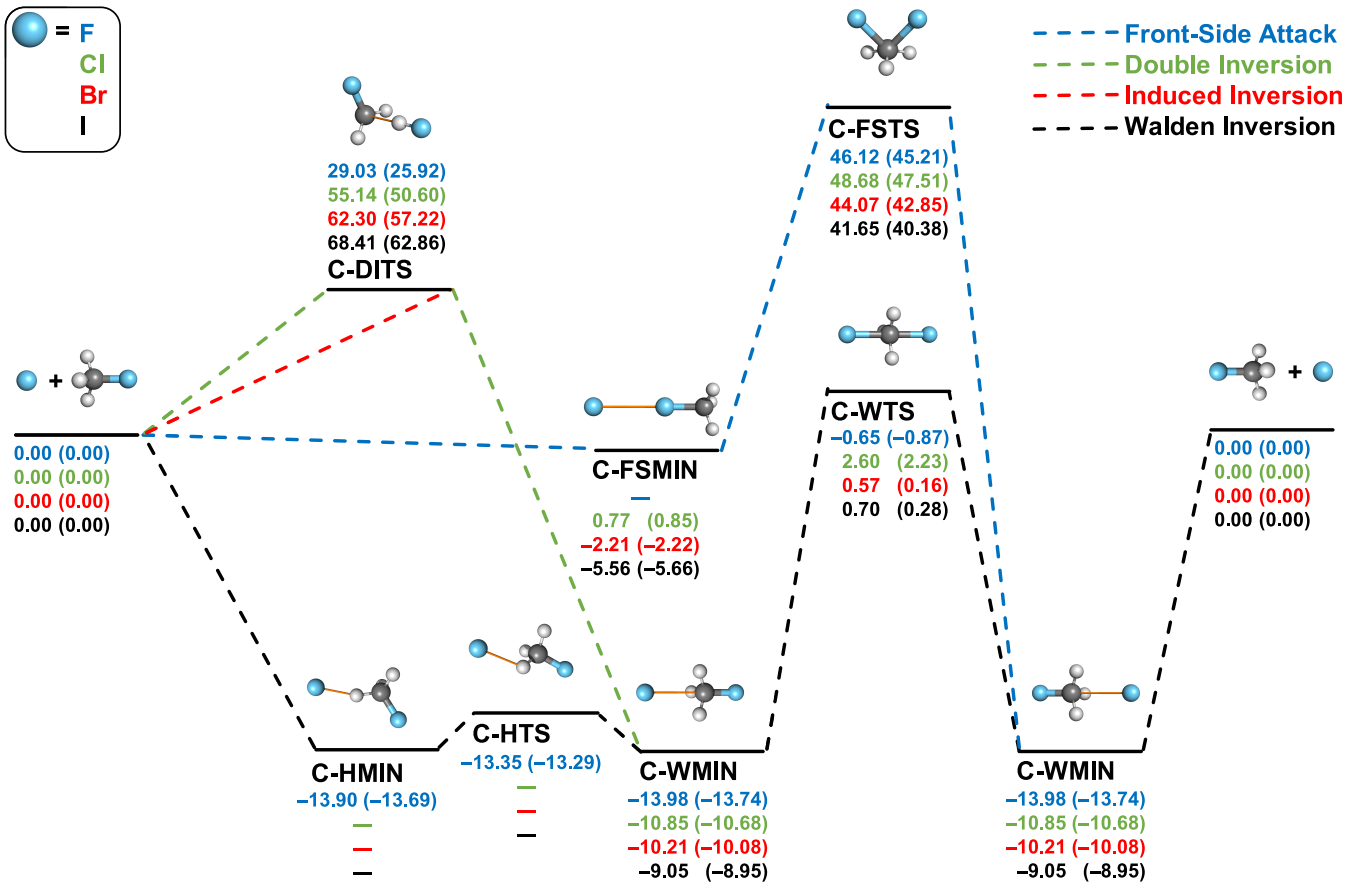

Figure 1. Pathways of X^- + CH_3X (X = F, Cl, Br, I) S_N2 reactions showing classical (adiabatic) relative energies in kcal/mol obtained at the CCSD(T)-F12b/aug-cc-pVQZ(-PP)//CCSD(T)-F12b/aug-cc-pVTZ(-PP) level of theory.

in some cases,[43,49,50] the energies are refined by the CCSD(T)/aug-cc-pVQZ level of theory.

In the present study, we report a comprehensive ab initio investigation of the identity and nonidentity X^- + SiH_3Y S_N2 reactions with X, Y = F, Cl, Br, I and compare them with the carbon-centered analogues. For the first time in the case of the Si-centered systems, we employ the explicitly correlated CCSD(T)-F12b method[57] to obtain benchmark structures, vibrational frequencies, and relative energies of the stationary points. In addition to the back-side and front-side attack, we also explore the possibility of double inversion in Si-centered S_N2 reactions. Furthermore, we determine the reaction enthalpies of several alternative product channels obtained by, for example, proton and halogen abstractions. These results may shape our fundamental knowledge of model ion−molecule reactions at carbon and silicon centers and guide future global potential energy surface developments and experimental and theoretical dynamics studies. The computational details are summarized in Section 2, the results are described and discussed in Section 3, and the paper ends with summary and conclusions in Section 4.

2. COMPUTATIONAL DETAILS

We determined optimized geometries and harmonic vibrational wavenumbers of the minima and saddle points of carbon- and silicon-centered X^- + CH_3Y/SiH_3Y [X, Y = F, Cl, Br, I] S_N2 reactions using the explicitly correlated coupled-cluster singles, doubles, and perturbative triples CCSD(T)-F12b method[57] with the augmented correlation-consistent aug-cc-pV*n*Z (*n* = D, T) basis sets.[58] In the case of Br and I, the corresponding aug-cc-pV*n*Z-PP basis sets are used employing effective core potentials considering relativistic effects.[59] Our highest-level electronic energy computations are performed using the aug-cc-pVQZ(-PP) basis sets[58,59] on the aug-cc-pVTZ(-PP) geometries. For open-shell systems (XY^- and CH_3/SiH_3), the unrestricted UCCSD(T)-F12b method[60] is used based on restricted open-shell Hartree−Fock[61] orbitals. All computations are carried out using the MOLPRO program package.[62]

3. RESULTS AND DISCUSSION

Figures 1 and 2 schematically present the most important pathways of the gas-phase identity and nonidentity halide ion and methyl-halide S_N2 reactions, respectively, in which the atomic number of the nucleophile is either equal to or smaller than the atomic number of the substituent. The considered pathways include Walden inversions, front-side attacks, induced inversions, and double inversions.

3.1. Pathways of Carbon-Centered S_N2 Reactions.

According to Figure 1, the energetically most-accessible Walden-inversion pathways of the identity reactions have low barriers in the case of Cl, Br, and I, whereas a small negative energy barrier is found for F (see C-WTS), surrounded by a symmetric double well in all cases. The ion-dipole complexes (C-WMIN) have decreasing stability from F to I with dissociation energies in the 9−14 kcal/mol range. Furthermore, a hydrogen-bonded low-energy minimum (C-HMIN) and a saddle point (C-HTS) connecting C-HMIN and

https://doi.org/10.1021/acs.jpca.1c07574
J. Phys. Chem. A 2021, 125, 9645−9657

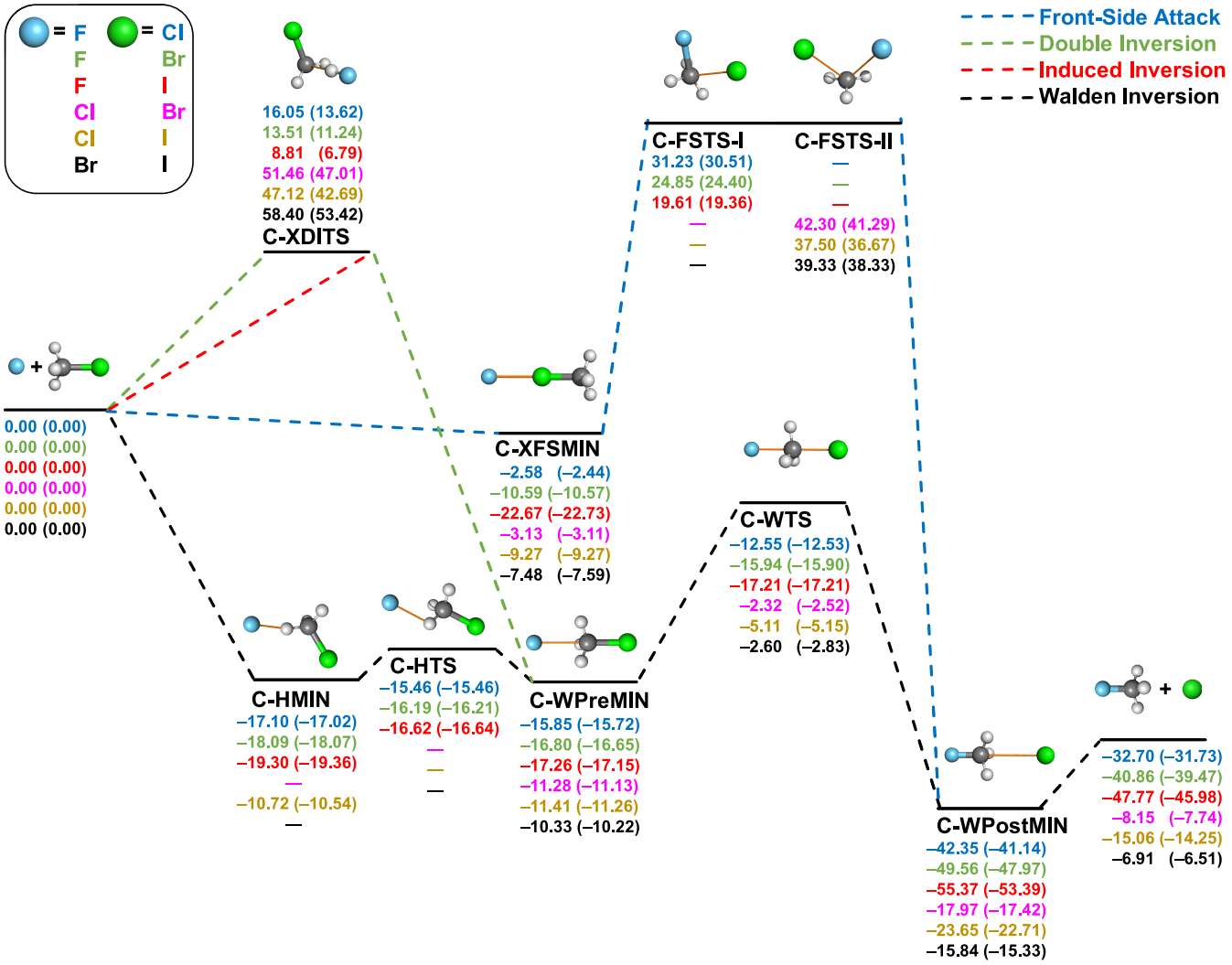

Figure 2. Pathways of $X^- + CH_3Y$ (X = F, Cl, Br; Y = Cl, Br, I) S_N2 reactions showing classical (adiabatic) relative energies in kcal/mol obtained at the CCSD(T)-F12b/aug-cc-pVQZ(-PP)//CCSD(T)-F12b/aug-cc-pVTZ(-PP) level of theory.

C-WMIN are present only for F. The energies of C-HMIN and C-WMIN are the same within 0.1 kcal/mol for the $F^- + CH_3F$ reaction. In contrast to the Walden-inversion pathway, the front-side attack mechanism goes through high-energy saddle points (C-FSTS) with barrier heights varying in the 40−46 kcal/mol range for all of the four cases. Except for F (and Cl), a front-side collision can yield a halogen-bonded complex, C-FSMIN, with D_0 dissociation energies of 2.22 and 5.66 kcal/mol for Br and I, respectively. For X = F, this stationary point cannot be found and for Cl and C-FSMIN has positive energy relative to the reactants. By comparing the relative energies of C-FSTSs and double-inversion transition states (C-DITSs), we can conclude that the double inversion is more accessible than the front-side pathway for the X = F identity reaction but less favorable for the other three cases.

Figure 2 shows the corresponding pathways for the exothermic nonidentity carbon-centered S_N2 reactions. Similar to the identity reactions, the back-side attack leads to a transition state, C-WTS, surrounded by a double well, but there are notable differences. Energetically, the F/Cl, F/Br, and F/I Walden-inversion transition states have deeper negative relative energies between −12.55 and −17.21 kcal/mol classically, whereas, for Cl/Br, Cl/I, and Br/I, the corresponding values are still negative, varying between −2.32 and −5.11 kcal/mol. The relative energies of C-WPostMINs also form two groups, deeper minima—relative to the reactants—for F/Cl, F/Br, and F/I and shallower negative energy minima for the other cases in accord with the trends in the exothermicities. The hydrogen-bonded low-energy saddle points, C-HTSs, consistent with the identity reactions are obtained only for the X = F reactions. In the cases where C-HTSs exist, they are below the corresponding C-WTSs and the hydrogen-bonded minima (C-HMINs) are deeper than the corresponding C-WPreMINs. Interestingly, the hydrogen-bonded Cl/I minimum can also be obtained, possibly, due to the low electronegativity of the I substituent; however, this C-HMIN is slightly above the corresponding C-WPreMIN. C-XFSMINs, similar to the C-FSMIN (in the identity reactions) structures, are minima with negative relative energies. In most cases, C-XFSMINs are significantly shallower than the corresponding C-HMINs and C-WPreMINs, except for F/I, where C-XFSMIN with $D_e(D_0)$ of 22.67(22.73) kcal/mol is the deepest minimum in the entrance channel. Thus, for F/I, the deep C-XFSMIN steers the reactants away from the reactive back-side attack configurations, thereby making the $F^- + CH_3I$ S_N2 reaction indirect as shown in the previous simulations and

https://doi.org/10.1021/acs.jpca.1c07574
J. Phys. Chem. A 2021, 125, 9645−9657

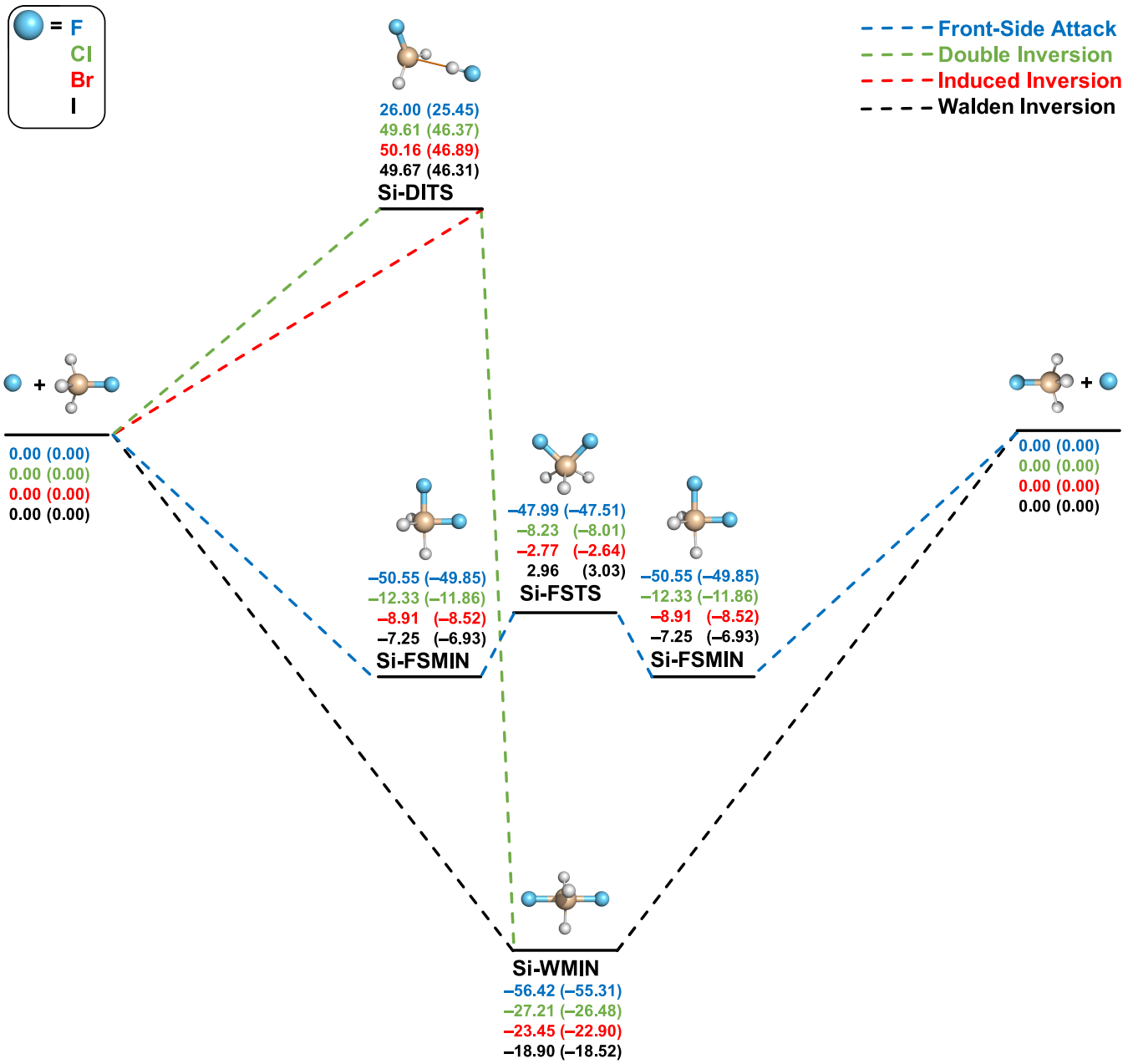

Figure 3. Pathways of X^- + SiH_3X (X = F, Cl, Br, I) S_N2 reactions showing classical (adiabatic) relative energies in kcal/mol obtained at the CCSD(T)-F12b/aug-cc-pVQZ(-PP)//CCSD(T)-F12b/aug-cc-pVTZ(-PP) level of theory.

experiments.[24,29] The nonidentity front-side attack transition states of F/Cl, F/Br, and F/I (C-FSTS-Is) compared to Cl/Br, Cl/I, and Br/I C-FSTS-IIs are very different geometrically. The former TSs possess the C_s point-group symmetry with four atoms (C, H, and two halogens) in its mirror planes and the latter three structures resembling more the TSs of the identity reaction counterparts with C_1 symmetry. Energetically, the double-inversion TSs (C-XDITSs) are more accessible to F-containing reactions than C-FSTS-Is, whereas the relative energies of Cl/Br, Cl/I, and Br/I C-XDITSs are higher than the relative energies of the corresponding C-FSTS-II saddle points. The lowest-energy retention pathways are found for the F/I reaction with classical (adiabatic) double-inversion and front-side attack barrier heights of 8.81(6.79) and 19.61(19.36) kcal/mol, respectively.

3.2. Pathways of Silicon-Centered S_N2 Reactions. As shown in Figures 3 and 4, the possible pathways of the gas-phase halide ion and silyl-halide S_N2 identity and nonidentity reactions are comparable to the carbon-centered counterparts, but the corresponding back- and front-side attack pathways and the underlying potential energy surfaces are qualitatively different.

In contrast to the carbon-centered reactions, the Walden-inversion pathways of the X^- + SiH_3Y S_N2 reactions do not go through transition states, and only a deep minimum connects the reactants and products with depths between 18.90 and 56.42 kcal/mol for identity reactions and from 27.85 to 82.73 kcal/mol classically for nonidentity reactions. The minima are significantly deeper for X = F (D_e = 56.42, 68.82, 75.08, 82.73 kcal/mol for Y = F, Cl, Br, I, respectively) than in the case of the other nucleophiles (D_e = 18.90−37.04 kcal/mol). On the

https://doi.org/10.1021/acs.jpca.1c07574
J. Phys. Chem. A 2021, 125, 9645−9657

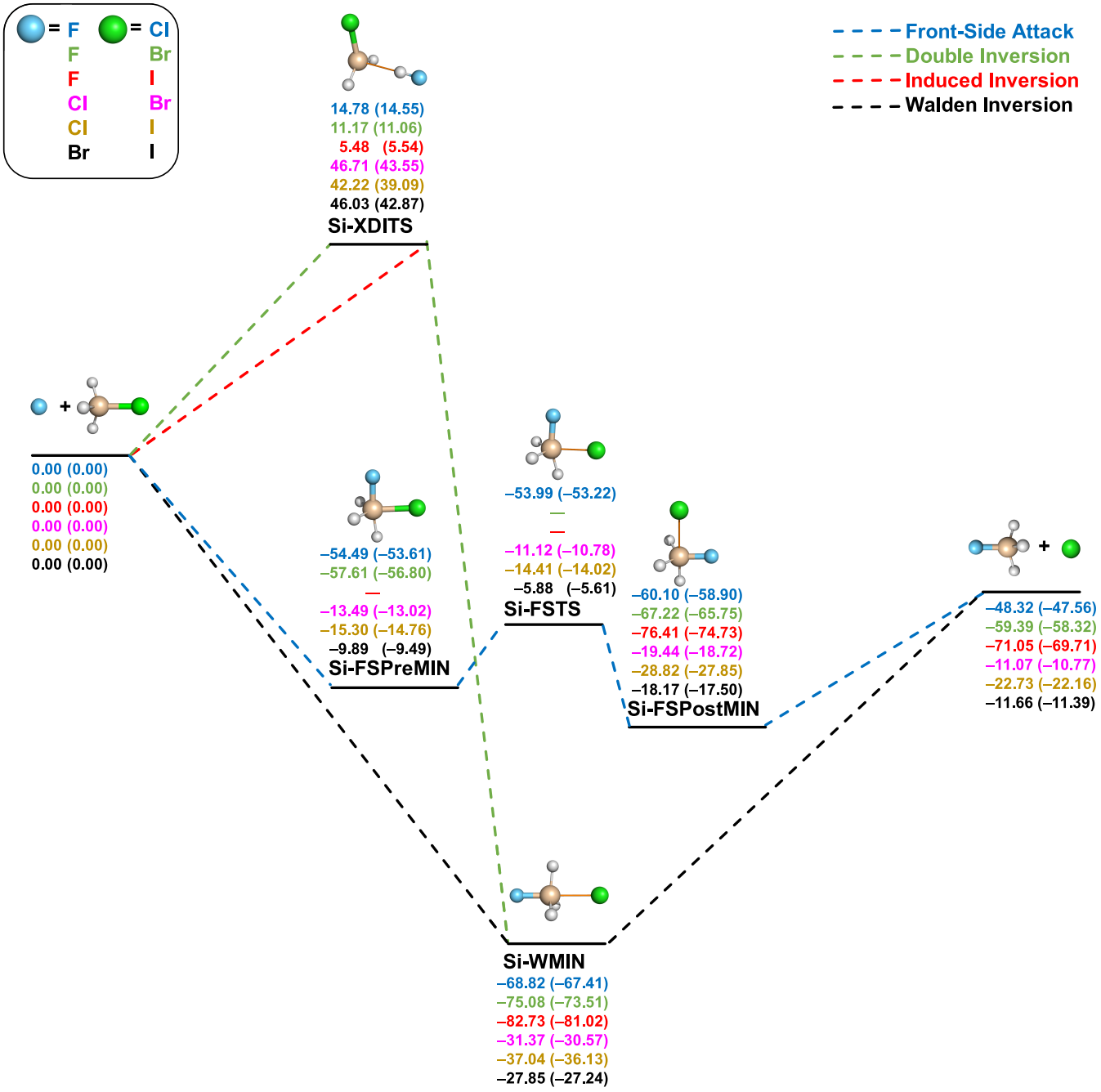

Figure 4. Pathways of X^- + SiH_3Y (X = F, Cl, Br; Y = Cl, Br, I) S_N2 reactions showing classical (adiabatic) relative energies in kcal/mol obtained at the CCSD(T)-F12b/aug-cc-pVQZ(-PP)//CCSD(T)-F12b/aug-cc-pVTZ(-PP) level of theory.

other hand, the front-side attacks on the Si center feature double-well potentials with saddle points (Si-FSTSs) separating minima (Si-FSMINs) symmetrically in the identity reactions and Si-FSPreMINs and Si-FSPostMINs for the nonidentity reactions. The TSs of the front-side attacks are geometrically like carbon-centered C-FSTSs in the identity reactions and comparable to C-FSTS-IIs of the nonidentity reactions. Energetically, the silicon-centered front-side attack pathways are accessible at lower energies than C-FSTSs, as Si-FSTSs are submerged in almost all cases, except for the I identity reaction, where the barrier height is a low positive value (2.96 kcal/mol classically). In some cases, especially for X = F, the Walden-inversion pathway is just slightly below the corresponding front-side attack retention path; thus, one may expect interesting competition between inversion and retention for silicon-centered S_N2 reactions, which may be investigated by dynamics simulations in the near future. The most similar pathways of the C- and Si-centered reactions are double inversions. The silicon-centered Si-DITSs (identity reactions) and Si-XDITSs (nonidentity reactions) are geometrically and energetically similar to the corresponding carbon-centered TSs. However, unlike for the F^- + CH_3Y systems, at the Si center, the positive double-inversion barriers are always above the corresponding Si-FSTSs.

3.3. Carbon-Centered Stationary Points. Figures 5 and 6 show the most important benchmark structural parameters of the stationary points (minima and transition states) of the potential energy surfaces of the carbon-centered identity- and

https://doi.org/10.1021/acs.jpca.1c07574
J. Phys. Chem. A 2021, 125, 9645−9657

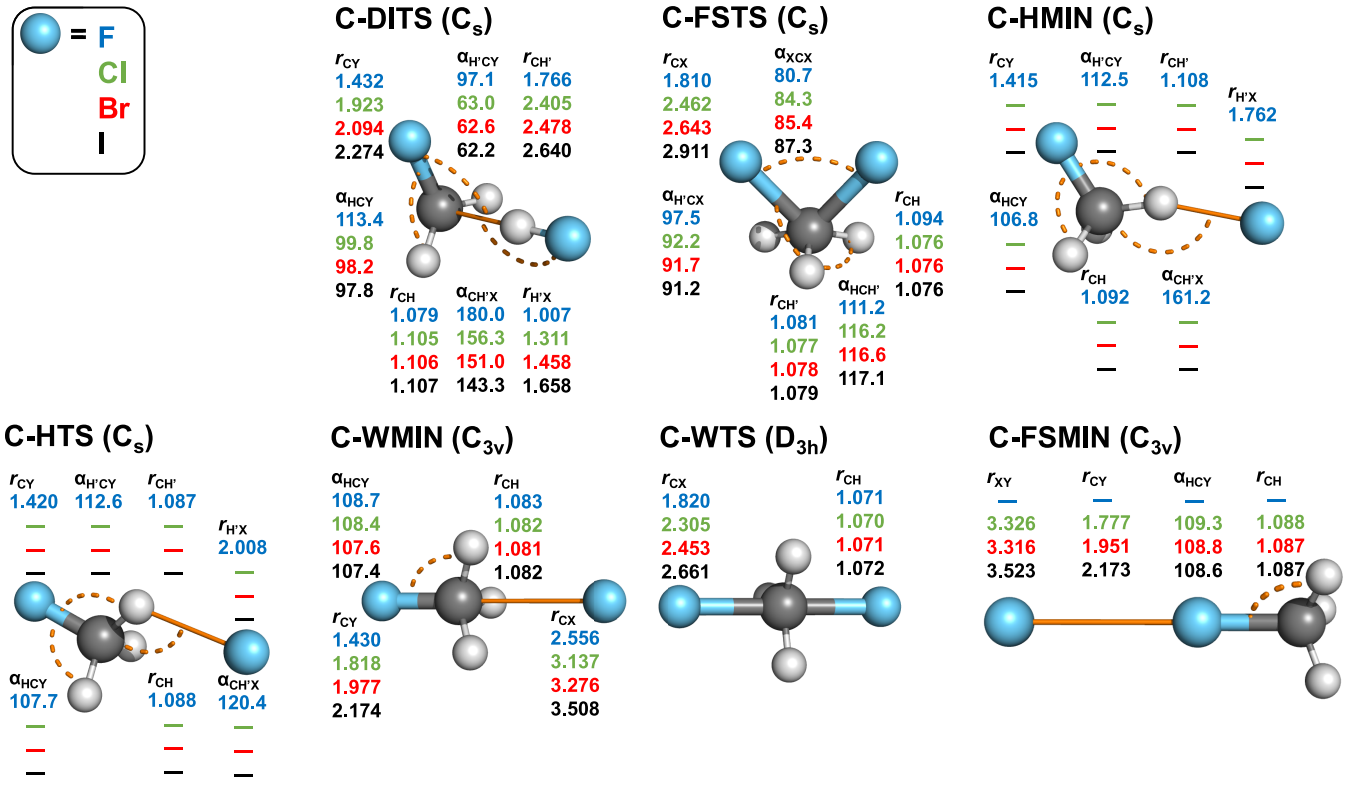

Figure 5. Structures and point groups of minima and saddle points of the X^- + CH_3X (X = F, Cl, Br, I) reactions optimized at the CCSD(T)-F12b/aug-cc-pVTZ(-PP) level of theory. Bond lengths and angles are given in angstroms and degrees, respectively. In the case of C_s structures, hydrogen atoms lying in the mirror plane are denoted by H′. In the subscripts, X and Y denote the nucleophile and substituent, respectively. X and Y are the same halogens but in different chemical environments.

nonidentity reactions, respectively. Contrary to Figures 1 and 2, C-YDITSs and C-YFSMINs, the endergonic nonidentity reaction counterparts of C-XDITSs and C-XFSMINs, respectively, are also presented in Figure 6.

As shown in Figure 5, all identity-reaction double-inversion TSs (C-DITSs), front-side attack TSs (C-FSTSs), and hydrogen-bonded C-HMIN and TS (C-HTSs) of the X = F reaction have C_s point-group symmetry. Front-side attack halogen-bonded complexes, C-FSMINs, possess a 3-fold C_{3v} symmetry. The point group of the Walden minima, C-WMINs, is also C_{3v} and the most symmetric structures are the C-WTSs belonging to D_{3h}.

Figure 6 shows the stationary points of the nonidentity reactions. The point-group symmetries of the double-inversion TSs (C-XDITSs and C-YDITSs) are, like in the identity reactions, all C_s. However, the F/Cl, F/Br, and F/I front-side TSs (C-FSTS-Is) are with the same point-group symmetry, C_s, as the identity reaction counterparts, and these geometries are structurally very different. In the case of identity reactions, the plane of reflection goes through the C atom and one of the hydrogens, whereas, in the case of the nonidentity C-FSTS-Is, the two halogens are in the plane as well. The true counterparts of the identity reaction C-FSTSs are C-FSTS-IIs, found for Cl/Br, Cl/I, and Br/I, with C_1 point-group symmetry. The symmetries of C-HMINs and C-HTSs are comparable to the corresponding minimum and the transition state found for the F identity reaction. Walden transition states (C-WTSs) have C_{3v} symmetry with collinear X−C−Y arrangements and structurally (and energetically) more like preminimum structures (C-WPreMINs) than C-WPostMINs.

Considering the structural parameters shown in Figures 5 and 6, we can observe that at C-WMIN, C-WPreMIN, and C-WPostMIN, the methyl-halide unit is only slightly perturbed and the C···X and C···Y distances are around 2.3−2.6, 3.1−3.2, 3.3−3.4, and 3.5 Å for X/Y = F, Cl, Br, and I, respectively. C-HMIN and C-HTS present for X = F, with H′···F distances of around 1.6−1.8 Å (HMIN) and 2.0 Å (HTS) and CH′F angles of 160−170° (HMIN), and 108−120° (HTS), where H′ denotes the hydrogen-bonded H atom. For the identity reactions, the C−X distances are stretched by 0.4−0.5 Å at C-WTS relative to the corresponding bond length in the CH_3X molecules. For the nonidentity reactions, the trends are similar but subtle differences can be observed; for example, the C−F distances are stretched by 0.6−0.8 Å. At the front-side minima, the CY···X atoms are collinear and the Y···X distance is around 2.3 Å for X/Y = F/Br and F/I and 2.5 Å for X/Y = F/Cl, whereas the halogen bond lengths are between 3 and 4 Å for X = Cl, Br, and I, in accord with the highest stability of the F/Br and F/I complexes. At the front-side attack TSs, the C−X and C−Y bonds are usually 0.1−0.2 Å longer than the corresponding distances in C-WTSs, except for the C−F bonds, which are shorter by 0.1−0.2 Å. Furthermore, the X−C−Y angles are in the 78−88° range for the front-side TSs, whereas the X−C−Y atoms are exactly collinear in C-WTSs. At the DITSs, the bond length of the HX fragment is close to the corresponding value in the HX molecule and the C···H interfragment distance is around 1.8 Å for X = F and 2.4−2.7 Å for X = Cl, Br, I, except for Cl/I.

3.4. Silicon-Centered Stationary Points. The benchmark stationary-point structures for the identity and nonidentity silicon-centered S_N2 reactions are shown in Figures 7

https://doi.org/10.1021/acs.jpca.1c07574
J. Phys. Chem. A 2021, 125, 9645−9657

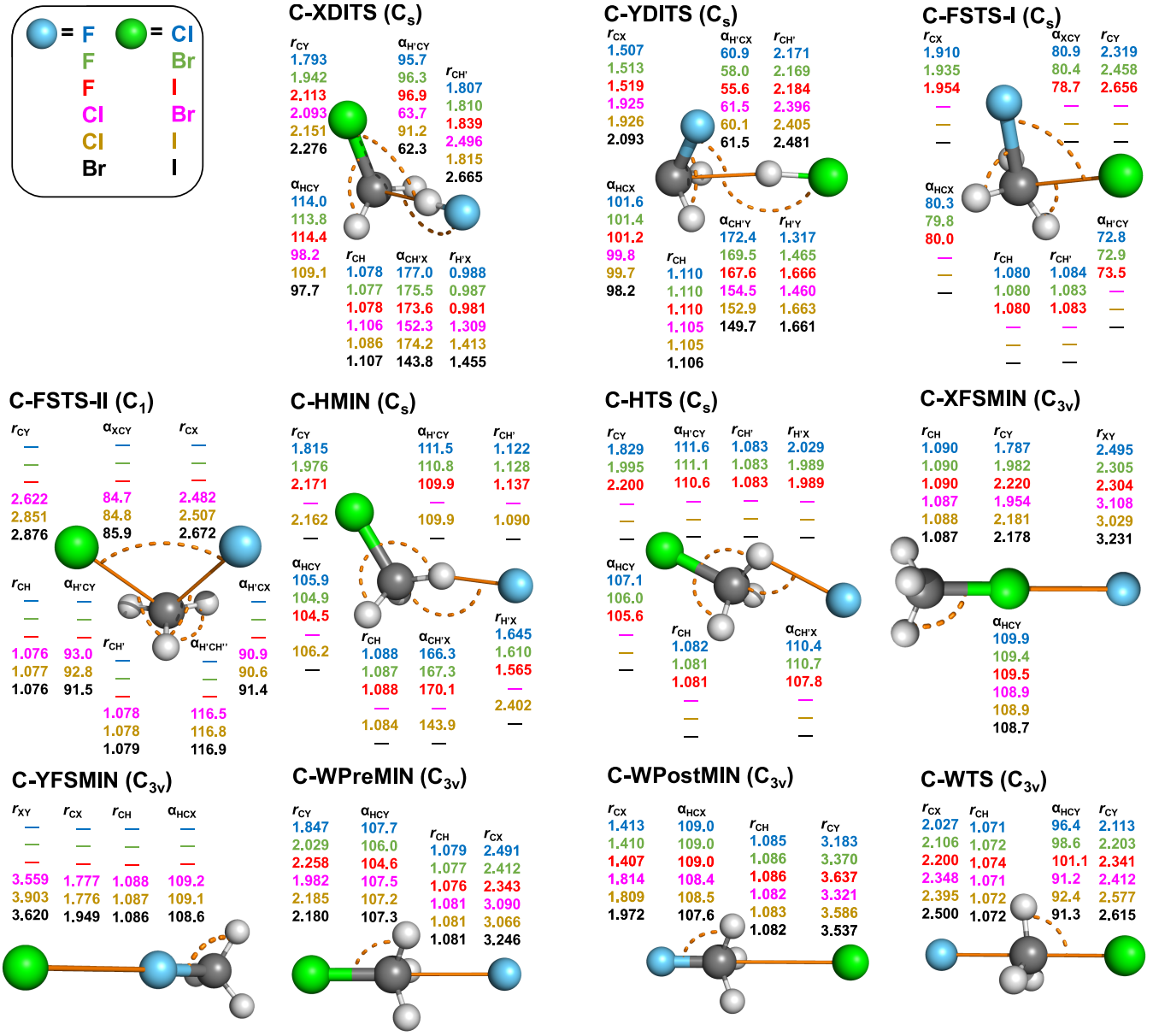

Figure 6. Structures and point groups of minima and saddle points of the X^- + CH_3Y (X = F, Cl, Br; Y = Cl, Br, I) reactions optimized at the CCSD(T)-F12b/aug-cc-pVTZ(-PP) level of theory. Bond lengths and angles are given in angstroms and degrees, respectively. In the case of C_s structures, hydrogen atoms lying in the mirror plane are denoted by H′.

and 8, respectively. In the case of the identity reactions, the structure of Si-WMINs is very similar to that of C-WTSs, i.e., both have a D_{3h} symmetry and the Si−X and C−X distances agree within about 0.1 Å. For the nonidentity reactions, the symmetries of Si-WMINs and C-WTSs are also the same (C_{3v}); however, unlike the reactant-like C-WTSs, the Si-WMINs are clearly product-like as the H−Si−X angle is greater than 90° and the Si−Y/Si−X distance ratios are significantly larger than the corresponding C−Y/C−X values. Hydrogen- and halogen-bonded complexes are not found for the X^- + SiH_3Y systems but there are front-side minima (Si-FSMIN, Si-FSPreMIN, and Si-FSPostMIN), which are not present for the C-centered reactions. Si-FSMINs of the identity reactions have C_s symmetry, where XXSiH′ atoms are in the symmetry plane, the X−Si−X angle is close to 90°, and the Si−H′ bond length is slightly stretched relative to the other two SiH distances. Si-FSPreMINs and Si-FSPostMINs of the nonidentity reactions have similar C_s structures as Si-FSMINs, but the Si−X distances are longer in Si-FSPreMINs than in Si-FSPostMINs, and the reverse is true for the Si−Y distances. FSTSs of the identity reactions have similar C_s structures at C and Si centers but they differ from Si-FSMINs because at FSTSs only the central atom and one of the hydrogen atoms are in the C_s plane. In the case of the nonidentity reactions, Si-FSTSs are nonsymmetric like the Cl/Br, Cl/I, and Br/I carbon-centered analogues. The X−Si−Y angles are in the 84−88° range for all of the Si-FSTS structures, similar to the C-centered FSTSs. The C- and Si-centered DITSs have similar C_s geometries; however, the C/Si−H′−X distances are significantly different in some cases. On the one hand, for X = F, the H′−F distance is close to the bond length of the HF molecule in both the C- and Si-centered cases, but the Si−H′ distance (∼2.4 Å) is substantially longer than the C−H′ distance (∼1.8 Å). On the other hand, for X = Cl, Br, I, the H′−X distances

https://doi.org/10.1021/acs.jpca.1c07574
J. Phys. Chem. A 2021, 125, 9645−9657

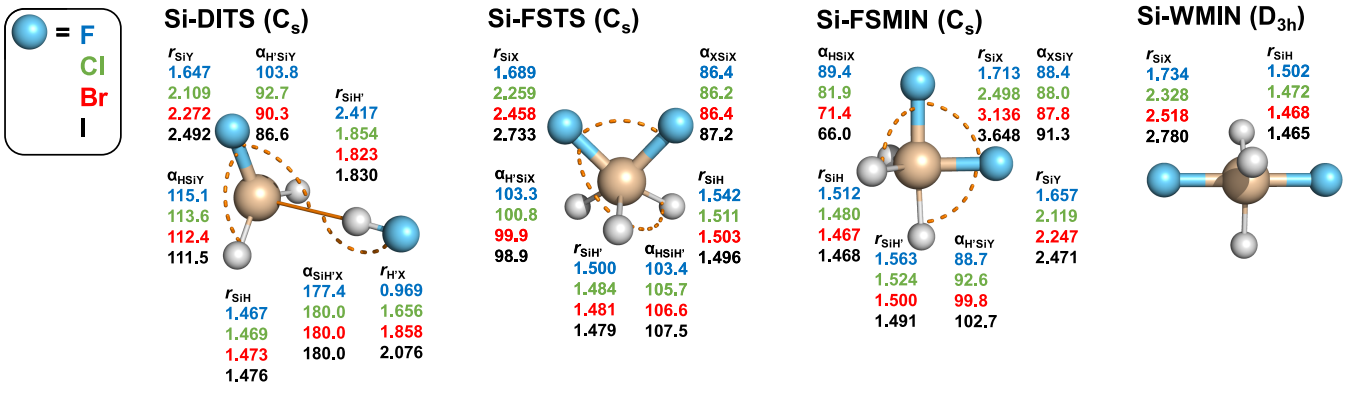

Figure 7. Structures and point groups of minima and saddle points of the X^- + SiH_3X (X = F, Cl, Br, I) reactions optimized at the CCSD(T)-F12b/aug-cc-pVTZ(-PP) level of theory. Bond lengths and angles are given in angstroms and degrees, respectively. In the case of C_s structures, hydrogen atoms lying in the mirror plane are denoted by H′. In the subscripts, X and Y denote the nucleophile and substituent, respectively. X and Y are the same halogens but in different chemical environments.

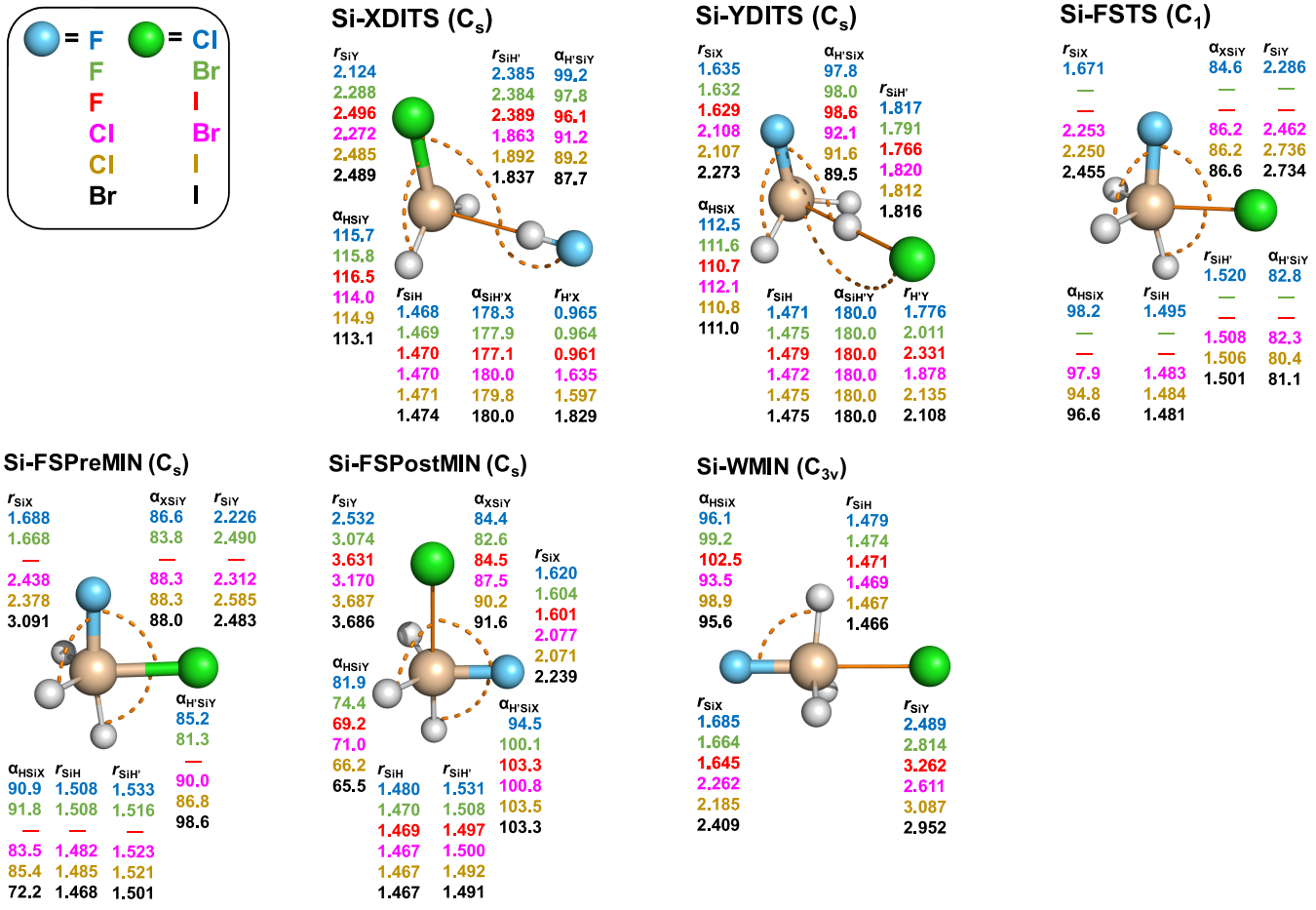

Figure 8. Structures and point groups of minima and saddle points of the X^- + SiH_3Y (X = F, Cl, Br; Y = Cl, Br, I) reactions optimized at the CCSD(T)-F12b/aug-cc-pVTZ(-PP) level of theory. Bond lengths and angles are given in angstroms and degrees, respectively. In the case of C_s structures, hydrogen atoms lying in the mirror plane are denoted by H′.

are stretched by about 0.4 Å relative to the corresponding distances of C-DITSs and HX molecules. Furthermore, the Si−X′ distances are only around 1.8−1.9 Å, whereas the corresponding C−X′ values are usually in the 2.4−2.7 Å range.

3.5. Reaction Enthalpies for Various Product Channels. We determined the reaction enthalpies corresponding to the various product channels of the X^- + CH_3Y and X^- + SiH_3Y reactions as shown in Tables 1 and 2, respectively. In addition to the S_N2 channel leading to Y^- + CH_3X/SiH_3X, we consider the proton abstraction (HX + CH_2Y^-/SiH_2Y^-), hydride substitution (H^- + CH_2XY/SiH_2XY), XH···Y^- complex-formation (XH···Y^- + $^1CH_2/^1SiH_2$), and halogen-abstraction (XY + CH_3^-/SiH_3^- and XY^- + CH_3/SiH_3) channels. For the X^- + CH_3Y reactions, the S_N2 channels are thermoneutral (X = Y) or exothermic and all other product channels are endothermic if the atomic number of X is less

https://doi.org/10.1021/acs.jpca.1c07574
J. Phys. Chem. A 2021, 125, 9645−9657

Table 1. Classical and Zero-Point Vibrational Energy Corrected (Adiabatic) Energies of $X^- + CH_3Y \rightarrow P + Q$ (X, Y = F, Cl, Br, I) Reaction Channels Obtained at the CCSD(T)-F12b/aug-cc-pVQZ(-PP)//CCSD(T)-F12b/aug-cc-pVTZ(-PP) Level of Theory in kcal/mol[a]

Q	Y^-	HX	H^-	XHY^-	XY	XY^-
P	CH_3X	CH_2Y^-	CH_2XY	$^1CH_2$	CH_3^-	CH_3
F/F	0.0(0.0)	42.2(37.8)	46.3(42.3)	55.3(47.5)	155.0(149.4)	87.0(81.5)
Cl/Cl	0.0(0.0)	68.6(63.0)	91.4(86.1)	83.5(73.6)	112.6(107.5)	57.8(53.1)
Br/Br	0.0(0.0)	74.6(68.7)	100.7(95.1)	88.7(78.9)	104.6(99.6)	46.4(41.9)
I/I	0.0(0.0)	78.8(72.6)	108.3(102.4)	95.8(85.9)	94.7(90.0)	37.0(32.8)
F/Cl	−32.7(−31.7)	28.7(24.8)	54.5(50.3)	43.6(37.6)	103.8(99.0)	52.7(48.1)
F/Br	−40.9(−39.5)	24.1(20.3)	56.1(52.0)	38.9(33.2)	91.1(86.5)	40.2(35.9)
F/I	−47.8(−46.0)	18.7(15.2)	58.3(54.2)	35.6(30.2)	73.3(69.1)	26.3(22.5)
Cl/Br	−8.2(−7.7)	63.9(58.5)	92.0(86.8)	80.0(71.8)	104.3(99.4)	47.6(43.2)
Cl/I	−15.1(−14.3)	58.6(53.4)	92.9(87.7)	77.2(69.5)	93.3(88.7)	37.7(33.6)
Br/I	−6.9(−6.5)	69.3(63.6)	101.3(95.7)	87.2(78.6)	95.0(90.3)	37.5(33.4)

[a]In the case of identity reactions, X and Y are the same; otherwise, Y denotes the halogen with the higher atomic number.

Table 2. Classical and Zero-Point Vibrational Energy Corrected (Adiabatic) Energies of $X^- + SiH_3Y \rightarrow P + Q$ (X, Y = F, Cl, Br, I) Reaction Channels Obtained at the CCSD(T)-F12b/aug-cc-pVQZ(-PP)//CCSD(T)-F12b/aug-cc-pVTZ(-PP) Level of Theory in kcal/mol[a]

Q	Y^-	HX	H^-	XHY^-	XY	XY^-
P	SiH_3X	SiH_2Y^-	SiH_2XY	$^1SiH_2$	SiH_3^-	SiH_3
F/F	0.0(0.0)	4.2(2.6)	−3.2(−6.0)	43.4(39.8)	164.5(160.7)	126.5(123.2)
Cl/Cl	0.0(0.0)	31.9(29.0)	50.1(46.5)	56.0(50.1)	106.6(103.0)	81.7(78.9)
Br/Br	0.0(0.0)	37.8(34.6)	62.0(58.0)	58.2(52.4)	95.6(92.0)	67.4(64.8)
I/I	0.0(0.0)	41.5(38.0)	74.3(70.1)	60.6(54.5)	81.0(77.5)	53.2(50.8)
F/Cl	−48.3(−47.6)	−8.0(−9.2)	−0.1(−2.9)	16.0(14.1)	97.7(94.4)	76.7(74.0)
F/Br	−59.4(−58.3)	−12.7(−13.7)	0.9(−1.9)	8.4(6.7)	82.1(79.0)	61.2(58.8)
F/I	−71.1(−69.7)	−18.5(−19.4)	2.3(−0.6)	0.3(−1.1)	59.6(56.7)	42.6(40.4)
Cl/Br	−11.1(−10.8)	27.2(24.5)	50.6(47.0)	49.6(45.3)	95.3(91.9)	68.6(66.0)
Cl/I	−22.7(−22.2)	21.3(18.8)	51.3(47.7)	42.0(38.2)	79.5(76.3)	53.9(51.6)
Br/I	−11.7(−11.4)	32.0(29.0)	62.5(58.5)	51.9(47.2)	81.3(77.9)	53.8(51.4)

[a]In the case of identity reactions, X and Y are the same; otherwise, Y denotes the halogen with the higher atomic number.

than or equal to that of Y. For X, Y = Cl, Br, I, halogen abstraction forming $XY^- + CH_3$ has the lowest endothermicity. For X = F, proton abstraction is thermodynamically more favored than FY^- formation, whereas for X = Cl, Br, I, proton abstraction is the second lowest-energy endothermic channel. Then, $XH\cdots Y^-$ formation opens usually with about 15 kcal/mol higher endothermicity than proton abstraction. Hydride substitutions are usually highly endothermic and have larger reaction enthalpies than the corresponding $XH\cdots Y^- + {}^1CH_2$ channels except for X/Y = F/F. In all cases, except for Br/I and I/I, the $XY + CH_3^-$ channels are the most endothermic; however, these product asymptotes correspond to excited singlet electronic states above the two doublet products ($XY^- + CH_3$), which can also be formed on a singlet potential energy surface. Furthermore, we note that even if the ground electronic state of CH_2 is triplet, we consider here the singlet $XH\cdots Y^- + {}^1CH_2$ products because these can be obtained with adiabatic dynamics.

For the $X^- + SiH_3Y$ reactions, the S_N2 channels are even more exothermic than the C-centered analogues. Here, proton abstraction is more favored than halogen abstraction in all cases. Moreover, proton abstraction is always the lowest-energy above S_N2, except for X/Y = F/F, where hydride substitution is exothermic becoming even more favored than the thermoneutral S_N2 channel. Furthermore, proton abstraction is also exothermic for X = F and Y = Cl, Br, I, though in these cases, S_N2 is even more exothermic. Unlike for the C-centered systems, $XY^- + SiH_3$ formation has always significantly higher reaction enthalpy than proton abstraction and in all cases, except for I/I, both hydride substitution and $XH\cdots Y^-$ formation are more favored than halogen abstraction. The $XH\cdots Y^- + {}^1SiH_2$ channel is above the $H^- + SiH_2XY$ asymptote for X/Y = F/F, Cl/Cl, F/Cl, F/Br and in all other cases, the former is less endothermic than the latter. (Note that unlike in the case of CH_2, singlet is the ground electronic state of SiH_2.) $XY + SiH_3^-$ is always the most endothermic channel, which corresponds to an excited electronic state similar to the carbon-centered analogue.

3.6. Basis Convergence. We studied the basis-set convergence of the CCSD(T)-F12b relative energies of all of the product channels and stationary points considered in the present study. The correlations of the aug-cc-pVDZ and aug-cc-pVTZ relative energies with the aug-cc-pVQZ reference data are shown in Figures 9 and 10 for the products and stationary points in the interaction region, respectively. For classical reaction heats, the aug-cc-pVDZ and aug-cc-pVTZ results agree with the aug-cc-pVQZ data with root-mean-square errors (RMSEs) of 1.10 and 0.44 kcal/mol, respectively. For the minima in the interaction regions, the corresponding RMSEs are 0.26 and 0.15 kcal/mol, whereas for the transition states the RMSE values are 0.42 and 0.21 kcal/mol, in order. Thus, one can see the fast basis-set convergence of the CCSD(T)-F12b method, often resulting in chemical accuracy even with the small aug-cc-pVDZ basis set. The larger RMSEs

https://doi.org/10.1021/acs.jpca.1c07574
J. Phys. Chem. A 2021, 125, 9645−9657

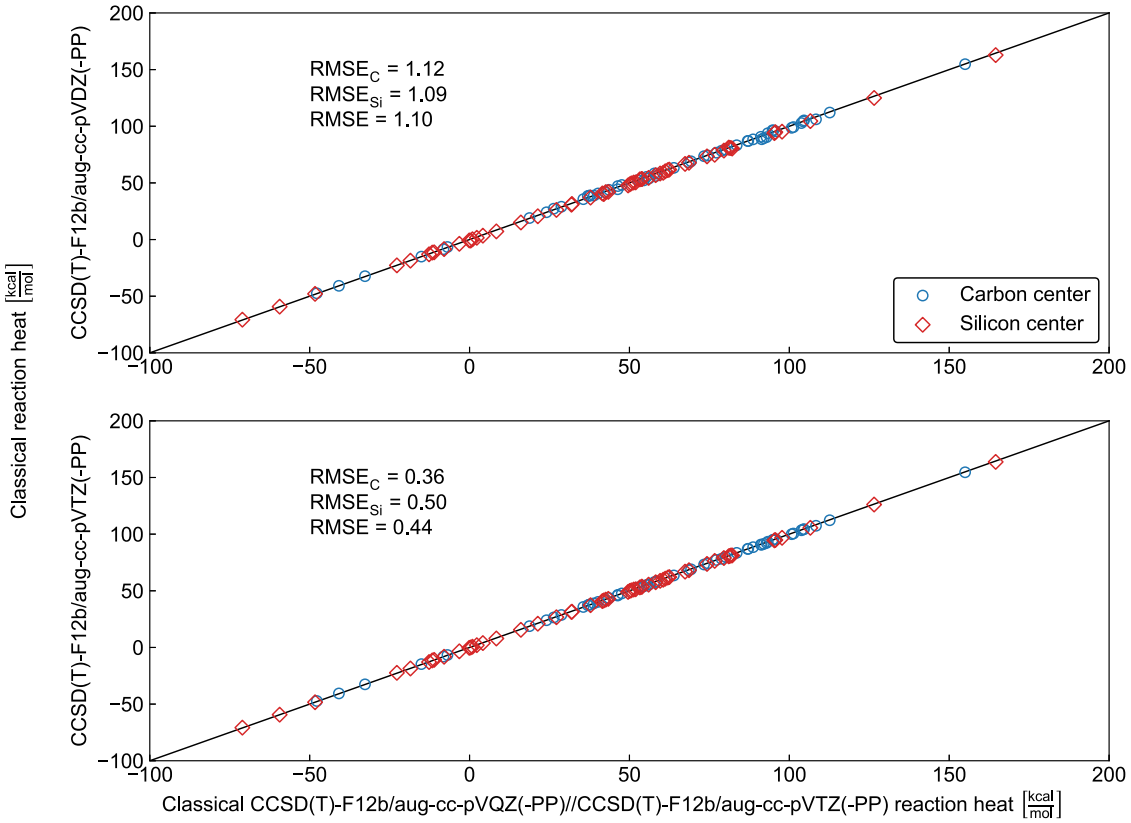

Figure 9. Comparison of classical reaction heats of $X^- + AH_3Y \rightarrow P + Q$ (X, Y = F, Cl, Br, I; A = C, Si; Q/P = Y^-/AH_3X, HX/AH_2Y^-, H^-/AH_2XY, XHY^-/AH_2, XY/AH_3^-, XY^-/AH_3) reactions obtained at the CCSD(T)-F12b/aug-cc-pV*n*Z(-PP) (*n* = D, T) and CCSD(T)-F12b/aug-cc-pVQZ(-PP)//CCSD(T)-F12b/aug-cc-pVTZ(-PP) levels of theory showing carbon-centered ($RMSE_C$), silicon-centered ($RMSE_{Si}$), and combined (RMSE) root-mean-square errors in kcal/mol.

for the reaction enthalpies than for the S_N2 stationary points in the interaction region can be explained by the fact that the reaction enthalpies cover a significantly wider energy range than the relative energies of the S_N2 stationary points and the electronic structures of the reactants and S_N2 stationary points are more similar than those of the reactants and products. Furthermore, larger transition-state RMSEs relative to those of the minima can also be understood knowing that the basis sets and ab initio methods usually perform better for minimum structures than for the electronically more problematic transition-state regions. Finally, comparing the basis-set convergence for the C- and Si-centered systems, only subtle difference can be seen as also shown in Figures 9 and 10.

4. SUMMARY AND CONCLUSIONS

Based on the recent knowledge accumulated on the reaction pathways of carbon-centered S_N2 reactions,[16,19,25,30,32] we present a comprehensive stationary-point characterization for the $X^- + CH_3Y$ and $X^- + SiH_3Y$ [X, Y = F, Cl, Br, I] S_N2 reactions using the explicitly correlated CCSD(T)-F12b method with the correlation-consistent aug-cc-pV*n*Z [*n* = D, T, Q] basis sets. Basis-set convergence tests are carried out, and the results show that the relative energies obtained in the present study are usually well within chemical accuracy. The potential energy surfaces of the C- and Si-centered S_N2 reactions are qualitatively different from several aspects. For C-centered reactions, the Walden-inversion process occurs on a double-well potential, where a central or a somewhat reactant-like transition state separates pre- and postreaction C_{3v} ion-dipole complexes. Furthermore, halogen-bonded C_{3v} front-side complexes and X = F hydrogen-bonded C_s complexes and transition states also exist in the entrance channels. Moreover, for X/Y = F/I, the front-side complex and, for F/Cl and F/Br, the hydrogen-bonded complexes correspond to the deepest minimum in the entrance channel. In the case of the Si-centered reactions, the Walden inversion proceeds on a single-well potential via a Walden TS-like central or somewhat product-like minimum and hydrogen- and halogen-bonded complexes cannot be found. The front-side attack retention pathways have high barriers at C centers, whereas the front-side attack transition states are submerged in most cases at Si centers. Unlike for the C-centered reactions, at the Si center, front-side minima with X−Si−Y angles close to 90° are found both in the entrance and exit channels. For the first time, we report double-inversion transition states for Si-centered S_N2 reactions, which are always above the reactant asymptotes and the front-side attack transition states. Thus, for Si-centered S_N2 reactions, front-side attack is clearly the dominant retention mechanism, which could be competitive with Walden inversion in some cases. At C centers, clearly Walden inversion is the major S_N2 mechanism in all cases and double inversion is the lowest-energy retention pathway for X = F.

In addition to the S_N2 pathways, we also determine the reaction enthalpies of various additional product channels, including proton abstraction, hydride substitution, $XH\cdots Y^-$ formation, and halogen abstraction. These additional channels are always, usually highly, endothermic for the C-centered reactions, whereas at the Si centers, proton abstraction, hydride substitution, and $XH\cdots Y^-$ formation are exothermic for some

https://doi.org/10.1021/acs.jpca.1c07574
J. Phys. Chem. A 2021, 125, 9645−9657

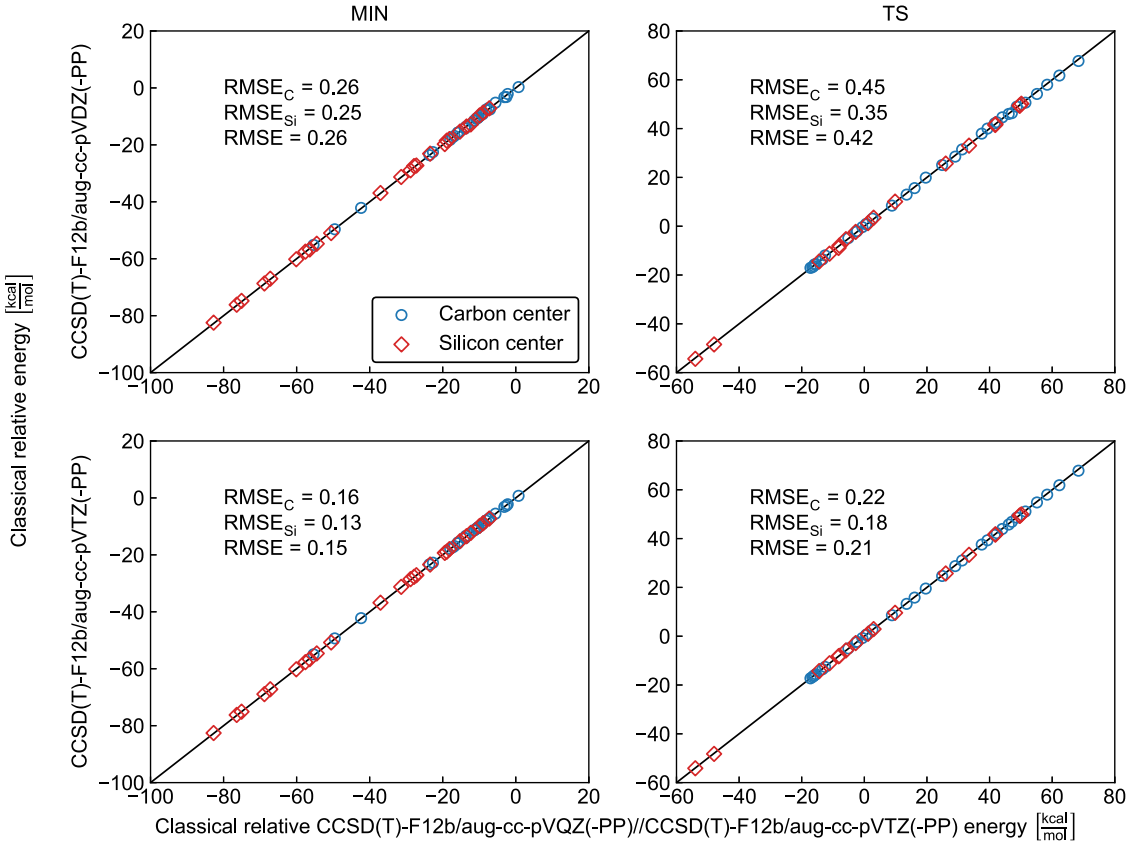

Figure 10. Comparison of classical relative energies of minima and saddle points in the interaction regions of the X^- + AH_3Y (X, Y = F, Cl, Br, I; A = C, Si) S_N2 reactions obtained at the CCSD(T)-F12b/aug-cc-pV*n*Z(-PP) (*n* = D, T) and CCSD(T)-F12b/aug-cc-pVQZ(-PP)//CCSD(T)-F12b/aug-cc-pVTZ(-PP) levels of theory showing carbon-centered ($RMSE_C$), silicon-centered ($RMSE_{Si}$), and combined (RMSE) root-mean-square errors in kcal/mol.

X = F cases. The knowledge of the reaction enthalpies of the various possible product channels could be useful for future global potential energy surface developments for these systems. Furthermore, as all of the different product channels produce different ions, the experimental detection of these reactions could be straightforward. The present results could guide and motivate such experiments and reaction dynamics simulations to uncover the central atom effects in ion−molecule reactions.

■ ASSOCIATED CONTENT

Supporting Information

The Supporting Information is available free of charge at https://pubs.acs.org/doi/10.1021/acs.jpca.1c07574.

Stationary point energies (XLSX)
Stationary point wavenumbers (XLSX)
Product energies (XLSX)
Product wavenumbers (XLSX)
Carbon-centered identity stationary points (TXT)
Carbon-centered nonidentity stationary points (TXT)
Silicon-centered identity stationary points (TXT)
Silicon-centered nonidentity stationary points (TXT)
Hydride substitution P C (TXT)
Hydride substitution P Si (TXT)
Proton abstraction P C (TXT)
Proton abstraction P Si (TXT)
Proton abstraction Q (TXT)
S_N2 P C (TXT)
S_N2 P Si (TXT)
XHY^- formation P C (TXT)
XHY^- formation P Si (TXT)
XHY^- formation Q (TXT)
XY^- anion formation P C (TXT)
XY^- anion formation P Si (TXT)
XY^- anion formation Q (TXT)
XY formation P C (TXT)
XY formation P Si (TXT)
XY formation Q (TXT)

■ AUTHOR INFORMATION

Corresponding Author

Gábor Czakó − *MTA-SZTE Lendület Computational Reaction Dynamics Research Group, Interdisciplinary Excellence Centre and Department of Physical Chemistry and Materials Science, Institute of Chemistry, University of Szeged, Szeged H-6720, Hungary;* orcid.org/0000-0001-5136-4777; Email: gczako@chem.u-szeged.hu

Authors

Attila Á. Dékány − *MTA-SZTE Lendület Computational Reaction Dynamics Research Group, Interdisciplinary Excellence Centre and Department of Physical Chemistry and Materials Science, Institute of Chemistry, University of Szeged, Szeged H-6720, Hungary*

Gyula Z. Kovács − *MTA-SZTE Lendület Computational Reaction Dynamics Research Group, Interdisciplinary Excellence Centre and Department of Physical Chemistry*

and Materials Science, Institute of Chemistry, University of Szeged, Szeged H-6720, Hungary

Complete contact information is available at: https://pubs.acs.org/10.1021/acs.jpca.1c07574

Notes

The authors declare no competing financial interest.

Supporting Information: Cartesian coordinates, absolute energies, and vibrational frequencies of the stationary points for the $X^- + AH_3Y \rightarrow P + Q$ (X, Y = F, Cl, Br, I; A = C, Si) reactions, where P denotes the product with the central atom, C or Si.

■ ACKNOWLEDGMENTS

The authors thank the National Research, Development and Innovation Office—NKFIH, K-125317, the Ministry of Human Capacities, Hungary, Grant 20391-3/2018/FEKUSTRAT, and the Momentum (Lendület) Program of the Hungarian Academy of Sciences for financial support. The authors also acknowledge KIFÜ for providing access to computational resource based in Hungary at Szeged.

■ REFERENCES

(1) Walden, P. Ueber die Gegenseitige Umwandlung Optischer Antipoden. *Ber. Dtsch. Chem. Ges.* **1896**, *29*, 133−138.

(2) Ingold, C. K. *Structure and Mechanisms in Organic Chemistry*; Cornell University Press: Ithaca, NY, 1953.

(3) Barlow, S. E.; Doren, J. M. V.; Bierbaum, V. M. The Gas-Phase Displacement Reaction of Chloride Ion with Methyl Chloride as a Function of Kinetic Energy. *J. Am. Chem. Soc.* **1988**, *110*, 7240−7242.

(4) Glukhovtsev, M. N.; Pross, A.; Radom, L. Gas-Phase Identity S_N2 Reactions of Halide Anions with Methyl Halides: A High-Level Computational Study. *J. Am. Chem. Soc.* **1995**, *117*, 2024−2032.

(5) Glukhovtsev, M. N.; Pross, A.; Radom, L. Gas-Phase Non-Identity S_N2 Reactions of Halide Anions with Methyl Halides: A High-Level Computational Study. *J. Am. Chem. Soc.* **1996**, *118*, 6273−6284.

(6) Viggiano, A. A.; Morris, R. A. Rotational and Vibrational Energy Effects on Ion-Molecule Reactivity as Studied by the VT-SIFDT Technique. *J. Phys. Chem. A* **1996**, *100*, 19227−19240.

(7) Clary, D. C.; Palma, J. Quantum Dynamics of the Walden Inversion Reaction $Cl^- + CH_3Cl \rightarrow ClCH_3 + Cl^-$. *J. Chem. Phys.* **1997**, *106*, 575−583.

(8) Yu, H.-G.; Nyman, G. An Application of the Rotating Line Umbrella Model to Quantum Dynamics of S_N2 Reactions. *Chem. Phys. Lett.* **1999**, *312*, 585−590.

(9) Ayotte, P.; Kim, J.; Kelley, J. A.; Nielsen, S. B.; Johnson, M. A. Photoactivation of the $Cl^- + CH_3Br$ S_N2 Reaction via Rotationally Resolved C-H Stretch Excitation of the $Cl^-{\cdot}CH_3Br$ Entrance Channel Complex. *J. Am. Chem. Soc.* **1999**, *121*, 6950−6951.

(10) Tachikawa, H.; Igarashi, M. A Direct ab-Initio Dynamics Study on a Gas Phase S_N2 Reaction $F^- + CH_3Cl \rightarrow CH_3F + Cl^-$: Dynamics of Near-Collinear Collision. *Chem. Phys. Lett.* **1999**, *303*, 81−86.

(11) Angel, L. A.; Ervin, K. M. Dynamics of the Gas-Phase Reactions of Fluoride Ions with Chloromethane. *J. Phys. Chem. A* **2001**, *105*, 4042−4051.

(12) Sun, L.; Song, K.; Hase, W. L. A S_N2 Reaction That Avoids Its Deep Potential Energy Minimum. *Science* **2002**, *296*, 875−878.

(13) Gonzales, J. M.; Pak, C.; Cox, R. S.; Allen, W. D.; Schaefer, H. F., III; Császár, A. G.; Tarczay, G. Definitive ab Initio Studies of Model S_N2 Reactions $CH_3X + F^-$ (X = F, Cl, CN, OH, SH, NH_2, PH_2). *Chem. - Eur. J.* **2003**, *9*, 2173−2192.

(14) Mikosch, J.; Trippel, S.; Eichhorn, C.; Otto, R.; Louderaj, U.; Zhang, J.-X.; Hase, W. L.; Weidemüller, M.; Wester, R. Imaging Nucleophilic Substitution Dynamics. *Science* **2008**, *319*, 183−186.

(15) Zhang, J.; Mikosch, J.; Trippel, S.; Otto, R.; Weidemüller, M.; Wester, R.; Hase, W. L. $F^- + CH_3I \rightarrow FCH_3 + I^-$ Reaction Dynamics. Nontraditonal Atomistic Mechanisms and Formation of a Hydrogen-Bonded Complex. *J. Phys. Chem. Lett.* **2010**, *1*, 2747−2752.

(16) Manikandan, P.; Zhang, J.; Hase, W. L. Chemical Dynamics Simulations of $X^- + CH_3Y \rightarrow XCH_3 + Y^-$ Gas-Phase S_N2 Nucleophilic Substitution Reactions. Nonstatistical Dynamics and Nontraditional Reaction Mechanisms. *J. Phys. Chem. A* **2012**, *116*, 3061−3080.

(17) Hennig, C.; Schmatz, S. Differential Reaction Cross Sections from Rotationally Resolved Quantum Scattering Calculations: Application to Gas-Phase S_N2 Reactions. *Phys. Chem. Chem. Phys.* **2012**, *14*, 12982−12991.

(18) Szabó, I.; Császár, A. G.; Czakó, G. Dynamics of the $F^- + CH_3Cl \rightarrow Cl^- + CH_3F$ S_N2 Reaction on a Chemically Accurate Potential Energy Surface. *Chem. Sci.* **2013**, *4*, 4362−4370.

(19) Xie, J.; Otto, R.; Mikosch, J.; Zhang, J.; Wester, R.; Hase, W. L. Identification of Atomic-Level Mechanisms for Gas-Phase $X^- + CH_3Y$ S_N2 Reactions by Combined Experiments and Simulations. *Acc. Chem. Res.* **2014**, *47*, 2960−2969.

(20) Xie, J.; Zhang, J.; Hase, W. L. Is There Hydrogen Bonding for Gas Phase S_N2 Pre-Reaction Complexes. *Int. J. Mass Spectrom.* **2015**, *378*, 14−19.

(21) Szabó, I.; Czakó, G. Revealing a Double-Inversion Mechanism for the $F^- + CH_3Cl$ S_N2 Reaction. *Nat. Commun.* **2015**, *6*, No. 5972.

(22) Szabó, I.; Czakó, G. Double-Inversion Mechanisms of the $X^- + CH_3Y$ [X,Y = F, Cl, Br, I] S_N2 Reactions. *J. Phys. Chem. A* **2015**, *119*, 3134−3140.

(23) Szabó, I.; Telekes, H.; Czakó, G. Accurate ab Initio Potential Energy Surface, Thermochemistry, and Dynamics of the $F^- + CH_3F$ S_N2 and Proton-Abstraction Reactions. *J. Chem. Phys.* **2015**, *142*, No. 244301.

(24) Stei, M.; Carrascosa, E.; Kainz, M. A.; Kelkar, A. H.; Meyer, J.; Szabó, I.; Czakó, G.; Wester, R. Influence of the Leaving Group on the Dynamics of a Gas-Phase S_N2 Reaction. *Nat. Chem.* **2016**, *8*, 151−156.

(25) Xie, J.; Hase, W. L. Rethinking the S_N2 Reaction. *Science* **2016**, *352*, 32−33.

(26) Olasz, B.; Szabó, I.; Czakó, G. High-Level ab Initio Potential Energy Surface and Dynamics of the $F^- + CH_3I$ S_N2 and Proton-Transfer Reactions. *Chem. Sci.* **2017**, *8*, 3164−3170.

(27) Ma, Y.-T.; Ma, X.; Li, A.; Guo, H.; Yang, L.; Zhang, J.; Hase, W. L. Potential Energy Surface Stationary Points and Dynamics of the $F^- + CH_3I$ Double Inversion Mechanism. *Phys. Chem. Chem. Phys.* **2017**, *19*, 20127−20136.

(28) Li, Y.; Wang, Y.; Wang, D. Y. Quantum Dynamics Study of the Potential Energy Minima Effect on Energy Efficiency for the $F^- + CH_3Cl \rightarrow FCH_3 + Cl^-$ Reaction. *J. Phys. Chem. A* **2017**, *121*, 2773−2779.

(29) Szabó, I.; Olasz, B.; Czakó, G. Deciphering Front-Side Complex Formation in S_N2 Reactions via Dynamics Mapping. *J. Phys. Chem. Lett.* **2017**, *8*, 2917−2923.

(30) Szabó, I.; Czakó, G. Dynamics and Novel Mechanisms of S_N2 Reactions on ab Initio Analytical Potential Energy Surfaces. *J. Phys. Chem. A* **2017**, *121*, 9005−9019.

(31) Tasi, D. A.; Fábián, Z.; Czakó, G. Rethinking the $X^- + CH_3Y$ [X = OH, SH, CN, NH_2, PH_2; Y = F, Cl, Br, I] S_N2 Reactions. *Phys. Chem. Chem. Phys.* **2019**, *21*, 7924−7931.

(32) Czakó, G.; Győri, T.; Olasz, B.; Papp, D.; Szabó, I.; Tajti, V.; Tasi, D. A. Benchmark ab Initio and Dynamical Characterization of the Stationary Points of Reactive Atom + Alkane and S_N2 Potential Energy Surfaces. *Phys. Chem. Chem. Phys.* **2020**, *22*, 4298−4312.

(33) Ji, X.; Zhao, C.; Xie, J. Investigating the Role of Halogen-Bonded Complexes in Microsolvated $Y^-(H_2O)_n + CH_3I$ S_N2 Reactions. *Phys. Chem. Chem. Phys.* **2021**, *23*, 6349−6360.

(34) Wester, R. Fifty Years of Nucleophilic Substitution in the Gas Phase. *Mass Spectrom. Rev.* **2021**, DOI: 10.1002/mas.21705.

(35) Meyer, J.; Tajti, V.; Carrascosa, E.; Győri, T.; Stei, M.; Michaelsen, T.; Bastian, B.; Czakó, G.; Wester, R. Atomistic

Dynamics of Elimination and Nucleophilic Substitution Disentangled for the F^- + CH_3CH_2Cl Reaction. *Nat. Chem.* **2021**, *13*, 977−981.
(36) Glukhovtsev, M. N.; Pross, A.; Schlegel, H. B.; Bach, R. D.; Radom, L. Gas-Phase Identity S_N2 Reactions of Halide Anions and Methyl Halides with Retention of Configuration. *J. Am. Chem. Soc.* **1996**, *118*, 11258−11264.
(37) Bento, A. P.; Bickelhaupt, F. M. Nucleophilicity and Leaving-Group Ability in Frontside and Backside S_N2 Reactions. *J. Org. Chem.* **2008**, *73*, 7290−7299.
(38) Papp, P.; Tajti, V.; Czakó, G. Numerical Separation of the Front-Side Attack and Double-Inversion Retention Pathways of S_N2 Reactions. *Chem. Phys. Lett.* **2020**, *755*, No. 137780.
(39) Liu, P.; Wang, D.; Xu, Y. A New, Double-Inversion Mechanism of the F^- + CH_3Cl S_N2 Reaction in Aqueous Solution. *Phys. Chem. Chem. Phys.* **2016**, *18*, 31895−31903.
(40) Liu, P.; Zhang, J.; Wang, D. Multi-Level Quantum Mechanics Theories and Molecular Mechanics Study of the Double-Inversion Mechanism of the F^- + CH_3I Reaction in Aqueous Solution. *Phys. Chem. Chem. Phys.* **2017**, *19*, 14358−14365.
(41) Shi, Z.; Boyd, R. J. The Laplacian of the Charge Density as a Probe of Reaction Paths and Reactivity: A Comparison of S_N2 Reactions at C and Si. *J. Phys. Chem. B* **1991**, *95*, 4698−4701.
(42) Bassindale, A. R.; Parker, D. J.; Taylor, P. G.; Auner, N.; Herrschaft, B. Modelling S_N2 Nucleophilic Substitution at Silicon by Structural Correlation with X-ray Crystallography and NMR Spectroscopy. *J. Organomet. Chem.* **2003**, *667*, 66−72.
(43) Bento, A. P.; Solà, M.; Bickelhaupt, F. M. Ab Initio and DFT Benchmark Study for Nucleophilic Substitution at Carbon (S_N2@C) and Silicon (S_N2@Si). *J. Comput. Chem.* **2005**, *26*, 1497−1504.
(44) Bento, A. P.; Bickelhaupt, F. M. Nucleophilic Substitution at Silicon (S_N2@Si) via a Central Reaction Barrier. *J. Org. Chem.* **2007**, *72*, 2201−2207.
(45) Pierrefixe, S. C. A. H.; Fonseca Guerra, C.; Bickelhaupt, F. M. Hypervalent Silicon versus Carbon: Ball-in-a-Box Model. *Chem. - Eur. J.* **2008**, *14*, 819−828.
(46) van Bochove, M. A.; Bickelhaupt, F. M. Nucleophilic Substitution at C, Si and P: How Solvation Affects the Shape of Reaction Profiles. *Eur. J. Org. Chem.* **2008**, 649−654.
(47) Ren, Y.; Wang, X.; Chu, S.-Y.; Wong, N.-B. Counter-Ion Effect in the Nucleophilic Substitution Reactions at Silicon: a G2M(+) Level Theoretical Investigation. *Theor. Chem. Acc.* **2008**, *119*, 407−411.
(48) Yang, Z.-Z.; Ding, Y.-L.; Zhao, D.-X. Theoretical Analysis of Gas-Phase Front-Side Attack Identity S_N2(C) and S_N2(Si) Reactions with Retention of Configuration. *J. Phys. Chem. A* **2009**, *113*, 5432−5445.
(49) Ding, Y.-L.; Mu, J.-R.; Gong, L.-D. Theoretical Study of Nucleophilic Identity Substitution Reactions at Nitrogen, Silicon and Phosphorus versus Carbon: Reaction Pathways, Energy Barrier, Inversion and Retention Mechanisms. *J. Chin. Chem. Soc.* **2013**, *60*, 327−338.
(50) Matsubara, T.; Ito, T. Quantum Mechanical and Molecular Dynamics Studies of the Reaction Mechanism of the Nucleophilic Substitution at the Si Atom. *J. Phys. Chem. A* **2016**, *120*, 2636−2646.
(51) Hupf, E.; Olaru, M.; Rat, C. I.; Fugel, M.; Hübschle, C. B.; Lork, E.; Grabowsky, S.; Mebs, S.; Beckmann, J. Mapping the Trajectory of Nucleophilic Substitution at Silicon Using a *peri*-Substituted Acenaphthyl Scaffold. *Chem. - Eur. J.* **2017**, *23*, 10568−10579.
(52) Rocha, M. V. J.; Smith, N. W. G.; Wolters, L. P.; de Cózar, A.; Fonseca Guerra, C.; Ramalho, T. C.; Bickelhaupt, F. M. Asymmetric Identity S_N2 Transition States: Nucleophilic Substitutionat α-Substituted Carbon and Silicon Centers. *Int. J. Mass Spectrom.* **2017**, *413*, 85−91.
(53) Hamlin, T. A.; Swart, M.; Bickelhaupt, F. M. Nucleophilic Substitution (S_N2): Dependence on Nucleophile, Leaving Group, Central Atom, Substituents, and Solvent. *ChemPhysChem* **2018**, *19*, 1315−1330.
(54) Bettens, T.; Alonso Giner, M.; De Proft, F.; Hamlin, T. A.; Bickelhaupt, F. M. Ambident Nucleophilic Substitution: Understanding NonHSAB Behavior through Activation Strain and Conceptual DFT Analyses. *Chem. - Eur. J.* **2020**, *26*, 3884−3893.
(55) Climent, C.; Feist, J. On the S_N2 Reactions Modified in Vibrational Strong Coupling Experiments: Reaction Mechanisms and Vibrational Mode Assignments. *Phys. Chem. Chem. Phys.* **2020**, *22*, 23545−23552.
(56) Fugel, M.; Dittmer, A.; Kleemiss, F.; Grabowsky, S. On the Role of Hydrogen Bonding in Gas-Phase S_N2 Reactions at Silicon. *J. Phys. Chem. A* **2021**, *125*, 4070−4078.
(57) Adler, T. B.; Knizia, G.; Werner, H.-J. A Simple and Efficient CCSD(T)-F12 Approximation. *J. Chem. Phys.* **2007**, *127*, No. 221106.
(58) Dunning, T. H., Jr. Gaussian Basis Sets for Use in Correlated Molecular Calculations. I. The Atoms Boron Through Neon and Hydrogen. *J. Chem. Phys.* **1989**, *90*, 1007−1023.
(59) Peterson, K. A.; Figgen, D.; Goll, E.; Stoll, H.; Dolg, M. Systematically Convergent Basis Sets with Relativistic Pseudopotentials. II. Small-Core Pseudopotentials and Correlation Consistent Basis Sets for the Post-*d* Group 16−18 Elements. *J. Chem. Phys.* **2003**, *119*, 11113−11123.
(60) Knizia, G.; Adler, T. B.; Werner, H.-J. Simplified CCSD(T)-F12 Methods: Theory and Benchmarks. *J. Chem. Phys.* **2009**, *130*, No. 054104.
(61) Hehre, W. J.; Radom, L.; Schleyer, P. V. R.; Pople, J. A. *Molecular Orbital Theory*; Wiley: New York, 1986.
(62) Werner, H.-J.; Knowles, P. J.; Knizia, G.; Manby, F. R.; Schütz, M.; Celani, P.; Györffy, W.; Kats, D.; Korona, T.; Lindh, R. et al. *MOLPRO, Version 2015.1, a Package of Ab Initio Programs*. http://www.molpro.net.

https://doi.org/10.1021/acs.jpca.1c07574
J. Phys. Chem. A 2021, 125, 9645−9657